Modeling the Absorbing Aerosol Index

Joyce Penner and Sophia Zhang
University of Michigan, Ann Arbor

Collaborator: Dr. Omar Torres
Goddard Space Flight Center

Abstract. We propose a scheme to model the absorbing aerosol index and improve the biomass carbon inventories by optimizing the difference between TOMS aerosol index (AI) and modeled AI with an inverse model. Two absorbing aerosol types are considered, including biomass carbon and mineral dust. A priori biomass carbon source was generated by Liousse et al. [1996]. Mineral dust emission is parameterized according to surface wind and soil moisture using the method developed by Ginoux [2000]. In this initial study, the coupled CCM1 and GRANTOUR model was used to determine the aerosol spatial and temporal distribution. With modeled aerosol concentrations and optical properties, we calculate the radiance at the top of the atmosphere at 340 nm and 380 nm with a radiative transfer model. The contrast of radiance at these two wavelengths will be used to calculate AI. Then we compare the modeled AI with TOMS AI. This paper reports our initial modelling for AI and its comparison with TOMS Nimbus 7 AI.

For our follow-on project we will model the global AI with aerosol spatial and temporal distribution recomputed from the IMPACT model and DAO GEOS-1 meteorology fields. Then we will build an inverse model, which applies a Bayesian inverse technique to optimize the agreement of between model and observational data. The inverse model will tune the biomass burning source strength to reduce the difference between modelled AI and TOMS AI. Further simulations with a posteriori biomass carbon sources from the inverse model will be carried out. Results will be compared to available observations such as surface concentration and aerosol optical depth.

1. Introduction

Anthropogenic aerosols have been identified as important to the radiative forcing of climate change. It is very important to quantify the magnitude of the forcing associated with anthropogenic aerosols in order to understand the total anthropogenic effect on the climate. Several studies have focused on the role of anthropogenic sulfate aerosols, their radiative forcing [Hansen et al. 1997, Mitchell et al. 1995] and their climate impact [Taylor and Penner 1994, Penner et al. 1996]. However, radiative forcing by biomass carbon aerosols is comparable on global scale [Penner et al. 1992, Penner et al. 1998a].

Carbonaceous aerosols, exclusive of carbonate carbon, are comprised of two classes of materials, black carbon (soot) and organic carbon. The two carbonaceous aerosols have different radiative properties. Black carbon is the principal solar radiation absorbing species in the atmosphere, while organic carbon is mainly scattering, like sulfate aerosols. Anthropogenic carbonaceous aerosols are mainly emitted by combustion sources and can be transported long distances over the oceans. The study by Penner et al., 1998a, suggests that carbonaceous aerosols perturb radiation balance and for most location and seasons, they together with sulfate aerosols lead to a net cooling. It has also been postulated that the absorption by carbonaceous aerosols might significantly alter both the vertical temperature structure of the atmosphere and the cloud fraction [Hansen et al., 1997, Ackerman et al. 2000]. Besides, scattering and absorption of solar radiation, carbonaceous aerosols also can influence climate through the indirect effect, where aerosols acts as cloud condensation nuclei (CCN) and determine the cloud droplet number concentration (CDNC), cloud albedo, precipitation and cloud lifetime. However, the magnitude of both the direct effect and indirect effect of biomass carbon aerosols remains very uncertain [IPCC, 2000]. One of such uncertainties associated with biomass carbonaceous aerosols lies in the uncertainty of biomass carbon emissions. The current biomass inventories we use are those developed by Liousse et al. [1996]. In this scheme biomass burning emissions are determined by the burnt area, vegetation density and efficiency of burning.

Satellite-based measurements provide a convenient and comprehensive method to characterize aerosol temporal and spatial distribution. Both AVHRR and the new MISER and MODIS aerosol data sets provide aerosol optical depth only over the water. Aerosol optical depth is a summation of the optical depth due to all aerosol types. Given that, it is very difficult to separate a specific aerosol from it, thus providing insufficient information to characterize biomass carbonaceous aerosols. Global distribution of UV-absorbing aerosols are obtained using measured differences between 340 and 380 nm radiance from the Nimbus 7 TOMS instrument over the time period

1979 - 1993. Using TOMS AI, the geographic distribution of absorbing aerosols such as carbonaceous aerosols, mineral dust and ash aerosols from volcanic eruptions have been described [Herman et al., 1997, Hsu et al. 1996]. Since TOMS AI only detects absorbing aerosols, this eliminates the uncertainties associated with scattering aerosols such as sea salt and sulfate aerosols associated with DMS. Therefore, use of the TOMS AI allows us a more accurate comparison for absorbing aerosols, such as biomass carbonaceous aerosols.

In this project, we first combine the chemical transport model and the radiative transport model to simulate AI for given a priori biomass and dust emissions. Once we have obtained AI from our model, an inverse model is used to optimize the difference between satellite measurements and model results by regularizing the biomass source strength. A posteriori biomass sources will be generated by the inverse model. Simulation with a posteriori biomass sources will be carried out and compared to ground based observations such as black carbon and organic carbon aerosol surface concentrations and satellite data such as optical depth at TOA. Below, we first introduce our chemical transport model and radiative transfer model. Then we describe how to simulate AI using the transport model and radiative transfer model. TOMS AI and modeled AI together with the inverse model are employed to obtain better biomass inventories.

2. Model Description

To obtain modeled AI, we need to calculate the 340 nm residue in our model. The 340 nm residue for Nimbus 7 instrument is defined as:

$$\Delta N = -100 \{\log_{10} [(I_{340}/I_{380})_{meas}] - \log_{10} [(I_{340}/I_{380})_{calc}]\}.$$

where I340 and I380 are the radiance at 340 and 380 nm, meas and calc represent measurements and model calculation respectively.

The aerosol spatial distribution must be known in order to carry out such a calculation. The 340 nm residue is also related to aerosol size distribution and aerosol optical properties. Our aerosol transport model will be used to compute the aerosol spatial and temporal distribution. A radiative transfer model will compute the radiance, given the atmosphere background gases and aerosol optical properties. We only consider the effect of aerosols on a Rayleigh atmosphere, because 320 - 400 nm is in near UV and the ozone absorption is weak and thus does not influence the interaction between aerosols and Rayleigh atmosphere.

2.1 Transport Model

The GRANTOUR model is a 3-D Lagrangian chemical transport model. The spatial resolution is approximately 4.5 o latitude by 7.5 o longitude and 14 vertical levels with eight in the troposphere. The NCAR Community Climate Model version 1. (CCM1) is a general circulation model with fixed sea surface temperature (SST). The GRANTOUR model uses the meteorological fields provided by CCM1 to calculate the transport and removal of aerosols. The aerosol concentration data is used by the CCM1 model to calculate radiation fields.

The first year simulation started with a clean back ground atmosphere. The model was spinned up for one year, only the data after the second year were used. The input species include biomass black carbon, biomass organic carbon and dust sources. The emissions of OC/ BC are directly adopted from the inventories developed by Liousse et al. [1996] which include savannah, forest, agriculture, domestic fires. (Table 1).

The dust source is generated interactively use the method by Ginoux et al. [2000]. The dust mobilization is parameterized based on wind speed at 10 meters, particle size and soil moisture. The size distribution for dust will be based on the work by d'Almeida [1987], or other observations if available.

In this simulation, biomass burning aerosols were injected from 700 mb to 400 mb while dust aerosols were injected at the surface. The mixing ratio of biomass carbon reach its maximum near 400 mb. However most of the dust aerosols reside below 800 mb. (Figure 1.) The column burden of biomass black carbon and dust aerosols

was shown in Figure 2. There is a seasonal variation of column burden for both of these two aerosols.

Table 1 Sources of carbonaceous aerosols from biomass burning

	Total biomass burned	Total smoke emissions (Tg/y) (Tgdm/y)	BC emissions (Tg/y)
Savannah	2682	21.7	2.2
Forest	1259	22.7	1.9
Agriculture fires	564	4.45	0.53
Wheat and other grains	192	2.06	0.22
Corn	41.1	0.46	0.04
Rice	218.5	1.15	0.19
Sugar cane	112.4	0.78	0.09
Domestic fires	869.5	11.07	1.01
Wood and bagasse	752.4	8.88	0.88
Charcoal	16.	0.16	0.02
Dung	101.1	2.02	0.10
Total	5374.5	59.9	5.64

Tgdm is teragrams of dry matter. Penner et al. 1998a

2.2 Aerosol model

The work by Radke et al. [1991] indicate that biomass smoke aerosols show little variation in smoke aerosol size from fire to fire or during a fire while near the source. Here we fit the dry aerosol size distribution with the measurements in the TRACE-A experiment by Anderson et al. [1996] with the sum of three log-normal distributions (Table 2.). For this initial study, we assume the relative humidity is 80% in the aerosol model. To account for the different optical properties for black carbon and organic carbon, we first calculate aerosol size distribution as a function of relative humidity and then combine optical properties using the volume average of the refractive index for each component. Because organic carbon is mainly scattering, in this calculation, for convenience, we assume the refractive index of organic carbon is the same as ammonium sulfate. The refractive indices for black carbon and dust are developed by d'Almeida et al. [1991] (Table 3). The refractive index at 340 nm is linearly interpolated from that at 300 nm and at 350 nm, while refractive index at 380 nm is linearly interpolated from that at 350 nm and at 400 nm. In the work by Penner et al. [1998a], they showed the single-scattering albedo for biomass carbonaceous aerosols based on Hardiman distribution and TRACE-A biomass experiment [Anderson et al. 1996] at relative humidity at 40%, 80% and 99%. The single scattering albedo for the two distribution near 300 nm and 400 nm is less than 3%. Biomass carbonaceous aerosols contain a varying ratio of black carbon to the total mass depending on the fire source [Liousse et al. 1996], therefore they have different single scattering albedo due to different sources.

The aerosol phase function is calculated using Mie Theory, which assumes spherical particles. Some biomass carbonaceous aerosols are hydrophilic. Absorbing liquid water tends to make the particle spherical. In the SCAR-B experiment in Brazil, particle shape was measured during different combustion phases [Martin et al. 1996]. The results indicate high variability of particle shape in the flaming phase and nearly spherical particle shape during

the smoldering phase. The asymmetric factor was less than 11%. Thus Mie Theory seems to be a good approximation for biomass carbonaceous aerosols. The shape of dust aerosols on the other hand, is seldom spherical. However, due to larger multiple scattering and increasing imaginary component in the refractive index in the near UV, the effect of non sphericity may produce less error than in the visible.

Table 2 An approximate fit to the average size distribution measured by Anderson et al. [1996]

Ni	ri (mm)	σ_i
0.9987	0.0774	1.402
1.306 x 10-3	0.3360	1.383
2.830 x 10-4	0.9577	1.425

Table 3 Aerosol optical properties

	ωo		Refractive index
Aerosol type	340 nm	380 nm	
Biomass Carbon	0.81	0.82	1.55-0.044i
Dust	0.74	0.75	1.53-0.08i

Refractive index is from d'Almeida et al. [1991].

2.3 Radiative Transfer Model

To calculate AI, we need to know the effect of aerosols on the near UV radiation field, specifically, we need to know the backscattered radiance at the top of atmosphere for the wavelengths 380 nm and 340 nm. The radiative transfer model we use is a modified version of the code developed by Herman and Browning [1965]. It includes the effects of multiple scattering. The higher-order scattering is assumed to take place in a plane parallel atmosphere.

The vertical distribution and aerosol optical properties are taken from the transport model and aerosol model respectively. A fixed surface reflectivity of 0.03 is used. In the future simulations, surface reflectivities at 340 nm and 380 nm are based on the monthly Lambert Equivalent Reflectivity (LER) of the earth surface at 380 nm which was developed by Herman and Celarier [1997] using Nimbus 7 TOMS measurements (Figure 4). As indicated in the TOMS measurements, the reflectivity of 0.03 is a typical value for vegetation covered land. For ocean surface, the reflectivity varies from 0.05 to 0.10. As indicated in the same work by Herman and Celarier, the difference of LER at 340 nm and 380 nm is less than 0.2%. Therefore, we assume a wavelength independent surface reflectivity for 340 nm -380 nm. The solar irradiance remains constant for the 340 -380 nm wavelength range, based on Schlesinger and Cebula [1992]. This assumption was also used for the TOMS retrieval. The sensitivity study for biomass carbon aerosols indicated that absorbing aerosol index is weakly dependent on the surface reflectivity (Figure 3).

Another input parameter is viewing geometry. In this study we assume a solar zenith angle of 40 o for all grid points. However, for our later study, we will use the TOMS Nimbus 7 level 2 data, which provide the viewing geometry for the measurements. In this preliminary implementation, the viewing angle for the satellite is assumed to be 0. The radiance will be calculated at the given viewing geometry for both 340 nm and 380 nm. Below are some input parameters for the radiative model:

Table 4 Parameters in the radiative transfer code.

	Rayleigh factor	King correction at TOA	Solar Flux angle	Solar Zenith angle	Viewingoptical depth
340 nm	0.7145	1.051	994.82	40 °	0 °
380 nm	0.4458	1.053	1109.31	40 °	0 °

Reference for Rayleigh optical depth and solar flux at TOA is McPeters et al. 1996,. Reference for King correction factor is Bates, 1984.

2.4 Simulating Aerosol Index

By combining the transport and radiative transport model, we can simulate AI for dust and biomass carbonaceous aerosols. The 3D aerosol distribution is computed before hand. The aerosol model and radiative transport model are coupled together. The dispatcher will call the aerosol model first. The aerosol model will read the aerosol concentration and computes the refractive index, extinction coefficient and aerosol optical depth. Then the code will call the radiative transfer model. The radiative transfer code will use the aerosol vertical distribution from the transport model and the refractive index and aerosol optical depth from the aerosol model. The code calculate the clearsky radiance at 380 nm (I 380), and 340 nm (I 340). Since clouds produce nearly zero residue, the presence of subpixel clouds does not affect the detection of aerosols, but it can reduce the amount of aerosols detected. The effect of cloud should be taken into account in later studies. As mentioned before, the TOMS AI is defined as 340 nm residue. Here we calculate the AI in the model by replacing the measured I340 and I380 in the definition for the TOMS AI with modeled radiance

$$\Delta N_{model} = -100 \{\log_{10} [(I_{340}/I_{380})_{model}] - \log_{10} [(I_{340}/I_{380})_{calc}]\}.$$

with $I380_{model} = I380_{calc}$

The (I_{340}/I_{380})calc is the radiance contrast calculated by the radiative transfer model for pure Rayleigh scattering atmosphere. It is calculated before hand and saved as a lookup table.

3. Model results

For this initial comparison, we only simulate aerosol index for January and July from 30 o W to 37.5 o E and 42 o S to 35 o N. The results are shown in Figure 5. The observed TOMS Nimbus 7 AI are shown in Figure 6.

In January, near the west coast of Africa, the observed AI is from 0.5 to 2.0. The modeled AI varies from 0.5 to 2.0, matches the observations in those region. The high AI (2.0 to 2.5) observed on the Africa coast near the Gulf Guinea is also present in the model results, although the area where AI is from 20 to 2.5 is smaller in the model. This might indicate that the biomass source is slightly weak. However, in the east Africa, TOMS AI is less than 0.1 while the model have higher value ranging from 0.5 to 2.0. In the column burden plot for biomass black carbon in January (Figure 2), the biomass aerosol cloud extends from west Africa to the east coast of Africa. The comparison of modeled AI with observations indicates that biomass burning strength is too strong in East Africa in January. The observed AI is from 2.0 to 2.5 near (14 o N, 14E o E). This high value is absent in the modeled results. This might indicate a missing biomass burning or dust source. Since this region is a large dry lake bed near Lake Chad which are associated with dust. The missing absorbing aerosol in the model might be dust.

In July, the plots of aerosol column burden and modeled AI shows a large difference with the observations.

In the Sahara and Sahel region of North Africa, the signal of absorbing aerosols is high from 2.5 to 4.0 in the TOMS observations. The Sahara dust is transported westward as far as to the Gulf of Mexico. However, in both the column burden plots (Figure 2) and modeled AI plots, this strong signal is absent. This might indicate that the dust source is too weak in the Sahara region in July and the westward transport is not strong enough in the transport model. Another reason for the discrepancies for the modeled AI and observations is TOMS AI is very sensitive to aerosol height. The coupled CCM1 and GRANTOUR model has a very coarse vertical resolution. The vertical transport of aerosols is weak in the model. [Zhang et al., 2001] For this reason, biomass carbon aerosols were injected at levels from 700 mb to 400 mb. However, dust aerosols were released at the surface. The vertical transport of dust aerosols could be too weak to bring the dust to enough height. Thus, the modeled AI might be smaller than the observations North Africa the Sahara and Sahel region. In the plot for modeled AI in July, there is a strong signal due to transport of absorbing aerosols from South America over the ocean. This transport is also present in the column burden plot for biomass black carbon in July (Figure 2). This transport is not observed in the TOMS AI plot for July. One reason is that the biomass aerosol reached its maximum near 400-500 mb. This might be valid for Africa biomass carbon. But observations in South America indicated that the height of biomass carbon is near 2-3 km and tends to be multiple-leveled. The larger height of biomass aerosols in South America can lead to overestimation of biomass carbon. Releasing biomass carbon at higher level also reduce the washout rate of the biomass aerosols in South America, thus increase the modeled AI. The modeled maximum of AI appears east of observations in South Africa near 15 o S. Examining the column burden plot for biomass black carbon (Figure 2) also suggest a larger column burden over the east coast of South Africa. This suggests that the biomass source in east South Africa is overestimated in the model.

4. Further Work

Global AI will be simulated and compared to the TOMS AI in each month. I will examine the spatial distribution and seasonal variation of modeled AI to see how well it matches the observations.

The coupled GRANTOUR and CCM1 model has very coarse resolution, which can introduce uncertainties in the comparison. In the future, the IMPACT model will be used in place of the coupled GRANTOUR and CCM1 model. The IMPACT model is an Eulerian model of transport, transformation and removal, whose spatial resolution is approximately 2 o latitude by 2.5 o longitude. The vertical resolution for this study is 20 sigma levels up to 10 hPa. In order to simulate the real atmosphere corresponding to the TOMS measurements period, the IMPACT model is driven by DAO GEOS meteorology data for the same time period. The DAO GEOS-1 Multiyear Assimilation (Reanalysis) product currently covers from March 1, 1980 through December 13, 1993. The Nimbus 7 TOMS products are also available from 1979 - 1993. So the DAO GEOS-1 Multiyear Assimilation provide a good coverage for the period of Nimbus 7 TOMS measurements.

The current version of code uses bulk refractive index for mixed dust and biomass carbon. The next step is to construct a sensitivity study which separates dust and biomass carbon. Sensitivity study with size distribution will be carried out to estimate the uncertainties. Since cloud can obscure the number of aerosols detected. A mechanism needs to be found to take cloud into account when we compare the modeled AI and TOMS AI.

The current is time consuming fro global calculation. However, since each grid point is independent with others. Therefore, the calculation of AI at each grid points can be distributed on several machines to speed up the code. The speed up is proportional to the number of machines (processors used) I will update the code so that it can be run on a distributed system.

Inverse modelling to be used to optimize the differences between TOMS AI and modeled AI by adjusting the a priori biomass sources. We can test the a posteriori biomass sources by comparing to observations such as surface concentration and aerosol optical depth.

Acknowledgements:

We would like to thank NASA fort its sponsorship of the GSSP program, which provided an opportunity for the collaboration of Sophia Zhang with Omar Torres during a summer stay. Funding was also provided by the NASA Aerosol Program.

References:

Ackerman, A. S., O. B. Toon, D. E. Stevens, A. J. Heymsfield, V. Ramanathan, E. J. Welton, 2000, Reduction of tropical cloudiness by soot. Science, 288,1042-1047

Anderson, B. E., W. B. Grant, G. L. Gregory, E. V. Browell, J. E. Collins, G. W. Sachse, D. R. Bagwell, C. H. Hudgins, D. R. Blake, and N. J. Blake, 1996, Aerosols from biomass burning over the tropical South Atlantic region:
Distribution and impacts, J. Geophys. Res., 101, 24117-24137

Balkanski, Y. J., D. J. Jacob, G. M. Gardner, W. M. Graustein, and K. K. Turekian, 1993, Transport and residence times of continental aerosols inferred from a global 3-dimensional simulation of 210Pb, J. Geophys. Res.
98, 20573- 20586

Bates, D. R., 1984, Rayleigh scattering by air, Space. Sci., 32, 785-790

Bergamaschi P., R. Hein, M. Heimann, P. J. Crutzen, 2000a, Inverse modeling of the global CO cycle, 1. Inversion of CO mixing ratios, J. Geophys. Res. 105, 1909-1927

Bergamaschi P., R. Hein, C. A. M. Brenninkmeijer, and P. J. Crutzen, 2000b, Inverse modeling of the global CO cycle, 2. Inversion of 13C/12C and 18O/16O isotope ratios, J. Geophys. Res. 105, 1929-1945

d'Almeida, G. A. 1991, Atmospheric aerosols: global climatology andradiative characteristics, A. Deepak Pub., Hampton, Va.

Ginoux, P., M. Chin, I. Tegen, J. Prospero, B. Holben, O. Dubovik, S. Lin, 2000, Sources and distributions of dust aerosols simulated with the GOCARTmodel, submitted

Giorgi, F., and W. L. Chameides, 1986, Rainout lifetimes of highly soluble aerosols and gases as inferred from simulations with a general circulation model, J. Geophys. Res., 91, 14367-14376

Hansen, J. E., M. Sato, A. Lacis, 1997, Radiative forcing and climate response. J. Geophys. Res., 102, 6831-6864

Hein, R., P. J. Crutzen, and M. Heimann, 1997, An inverse modeling approach
to investigate the global atmospheric methane cycle, Global Biogeochem.
Cycles, 11, 43-76

Herman, B. M. and S. R. Browning, 1965, A Numerical Solution to the Equation of Rdiative Tranfer, J. Atmos. Sci. 22, 559-566.

Herman, J. R., P. K. Bhartia, O. Torres, C. Hsu, C. Seftor, and E. Celarier, 1997, Global distribution of UV-absorbing aerosols from Nimbus-7/TOMS data, J. Geophys. Res., 102, 16911-16922

Herman, J. R., and E. Celarier, 1997, Earth's surface reflectivity climatology at 340-380 nm from TOMS data., J. Geophys. Res. 102, 28003-28012

Hsu, N. C., J. R. herman, P. K. Bhartia, C. J. Seftor, O. Torres, A. M. Thompson, J. F. Gleason, T. F. Eck, and B. N. Holben, 1996, Detection of biomass burning smoke from TOMS measurements, J. Geophys. Res. Lett., 23, 745-748

Hsu, N. C., J. R. Herman, O. Torres, B. N. Holben, D. Tanre, T. F. Eck, A. Smirnov, B. Chatenet and F. Lavenu, 1999, Comparisons of the TOMS aerosol index with Sun-photometer aerosol optical thickness: Results and applications, J. Geophys. Res. 104, 6269-6279

Intergovernmental Panel on Climate Change (IPCC) (2000) World Meteorological Office, United Nations Environmental Programme, Aerosols and Radiative Forcing, Report to IPCC from the Scientific Assessment Working

Group
Jacob, D. J., and S. C. Wofsy, 1990, Budgets of reactive nitrogen, hydrocarbons, and ozone over the Amazon forest during the wet season, J. Geophys. Res., 95, 16737-16754
Joiner, J., P. K. Bhartia, R. P. Cebula, E. Hilsenrath, and R. D. McPeters, 1995, Rotational Raman scattering (ring effect) in satellite backscatter ultraviolet measurements, Appl. Opt., 34, 4513-4525
Lin, S. J. and R. B. Rood, 1996, Multidimensional flux-form semi-Lagrangian transport schemes, Mon. Wea. Rev., 124, 2046-2070
Liou, K. N., Q. Fu, and T. P. Ackerman, 1988, A simple formulation of the delta-four-stream approximation for the radiative transfer parameterization., J. Atmos. Sci., 45, 1940-1947
Liousse, C., J. E. Penner, C. Chuang, J. J. Walton, and H. Eddleman, 1996, A global three-dimensional model study of carbonaceous aerosols, J. Geophys. Res., 101, 19411-19432
Martins, J. V., P. V. Hobbs, R. E. Weiss, and P. Artaxo, 1996, Shapes of smoke particles from biomass burning in Brazil, SCAR-B Proceedings, edited by V. W. J. H. Kirchhoff, Transtec Ed., Sao Paulo, Brazil
McPeters, R. D., et al., Nimbus 7 total ozone mapping spectrometer (TOMS) data products users' guide, NASA Ref. Publ. 1384, 1996
Penner, J. E., R. E. Dickinson, and C. A. O'Neill, 1992, Effects of Aerosol from biomass burning on the global radiation budget, Science, 256,1432-1434
Penner, J. E. C. C. Chuang and K. Grant, 1998a, Climate forcing by carbonaceous and sulfate aerosols, Climate Dynamics, 14, 839-851
Penner, J. E., D. Bergmann, J. J. Walton, D. Kinnison, M. J. Prather, D. Rotman, C. Price, K. E. Pickering, S. L. Baughcum, 1998b, An evaluation of upper tropospheric NOx with two models, J. Geophys. Res., 103, 22097-22114
Radke, L. F., D. A. Hegg, P. V. Hobbs, J. D. Nance, J. H. Lyons, K. K. Laursen, R. E. Weiss, P. J. Riggan, and D. E. Ward, 1991, Particulate and trace gas emissions from large biomass fires in North America, in Global Biomass Burning: Atmospheric, Climatic, and Biospheric Implications, edited by J. S. Levine, chap. 28, 209-224, MIT Press, Cambridge, Mass.
Schlesinger B. M. and R. P. Cebula, 1992, Solar variation 1979-1987 estimated from an empirical model for changes with time in the sensitivity of the solar backscatter ultraviolet instrument, J. Geophys. Res., 97, 10119-10134
Taranrola, A., and B. Valette, 1980a, Generalized nonlinear inverse problems solved using the least square criterion, Rev. Geophys., 20, 219-232
Taranrola, A., and B. Valette, 1980b, Inverse problems-Quest of information, J. Geophys., 50, 159-170
Taylor, K. E.,a nd J. E. Penner, 1994, Response of the climate system to atmospheric aerosols and greenhouse gases, Nature, 369, 734-737
Wesely, M. L., 1989, Parameterization of surface resistances to gaseous dry deposition in regional-scale numerical models, Atmos. Environ., 23, 1293-1304
Walcek, C. J., R. A. Brost, J. S. Chang, and M. L. Wesely, 1986, SO2, sulfate, and HNO3 deposition velocities computed using regional landuse and meteorological data, Atmos. Environ., 20, 949-964

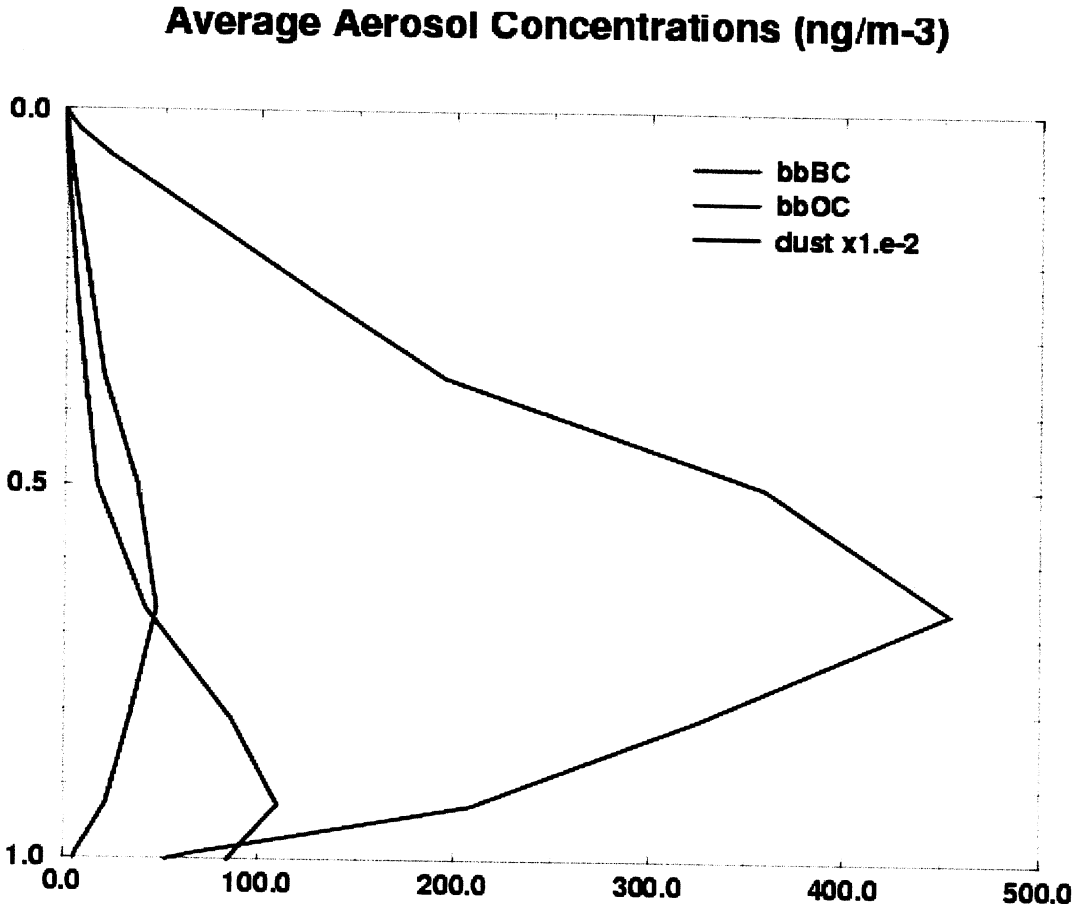

Figure 1. Averaged concentration of biomass black carbon (bbBC), biomass organic carbon (bbOC) and dust. Dust concentration was scaled by 1.e-2. Y-axis is the sigma level. X-axis is aerosol concentration.

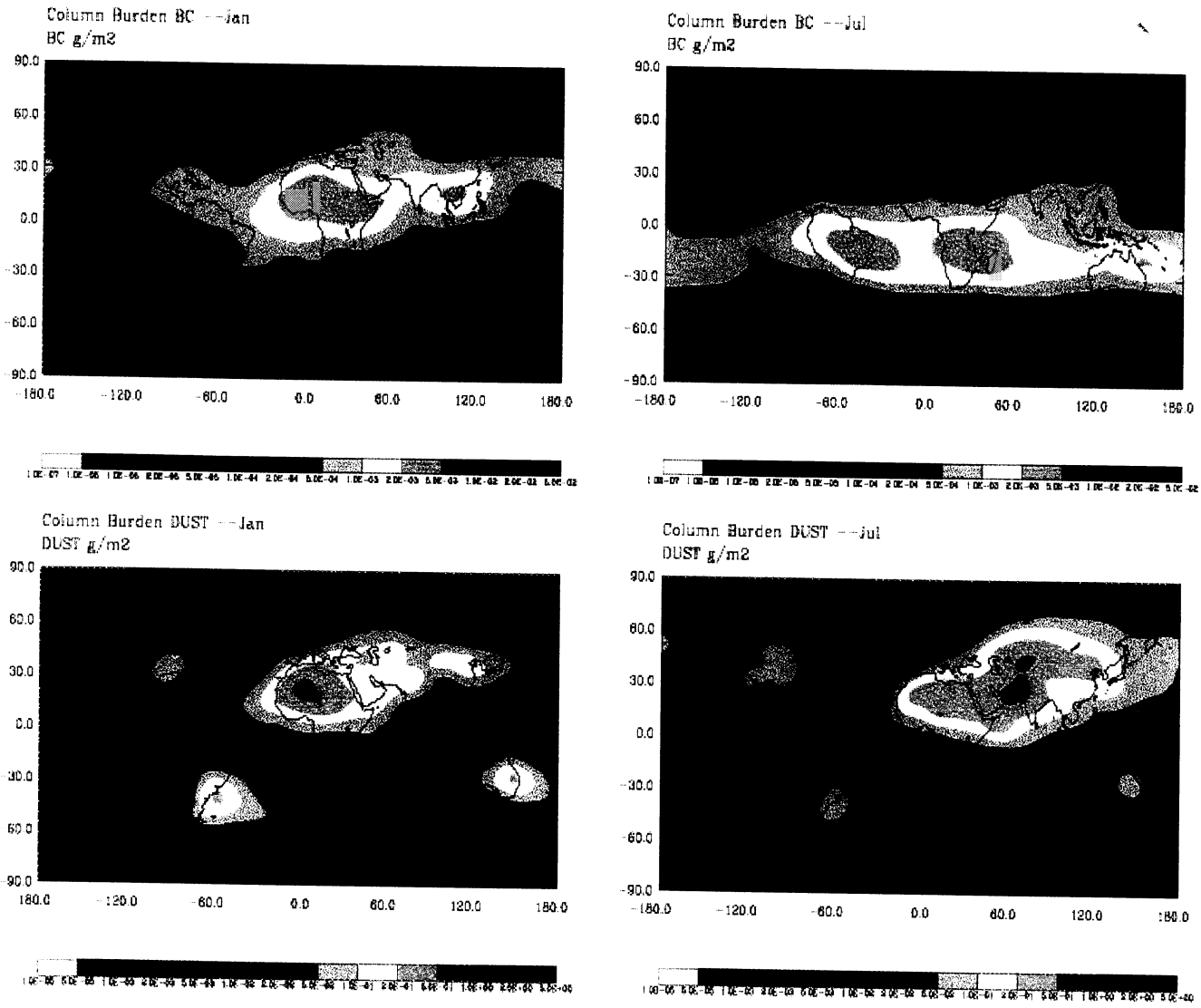

Figure 2. Biomass black carbon (BC) and dust column burden in January and July.

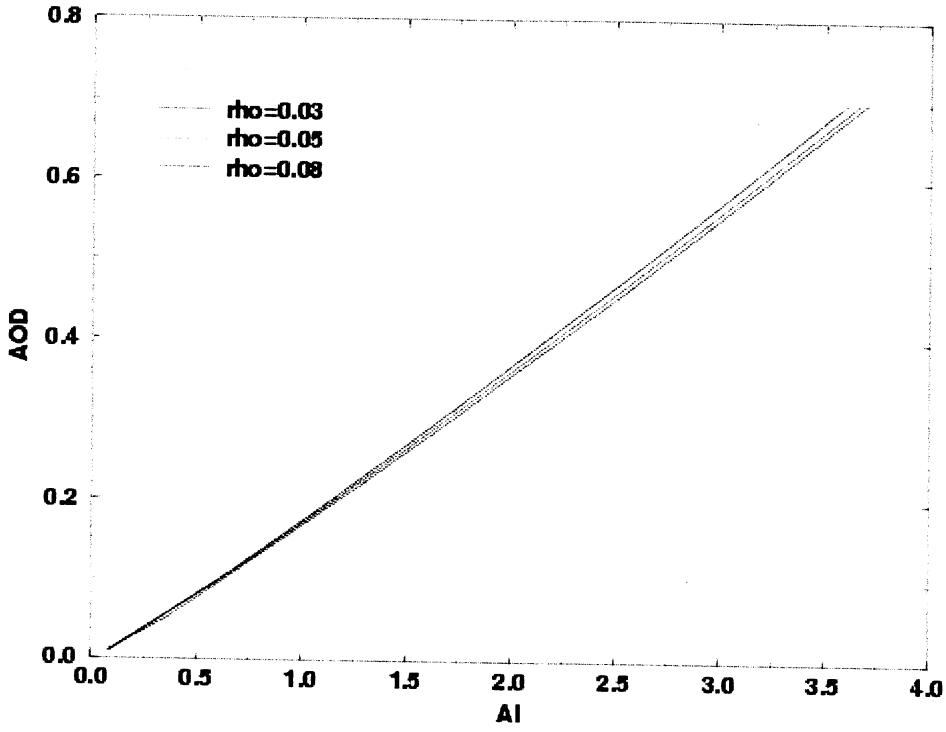

Figure 3. Relationship of aerosol optical depth (AOD) at 380 nm and Aerosol Index (AI). The three lines are for surface reflectivity is equal to 0.03, 0.05 and 0.08 respectively

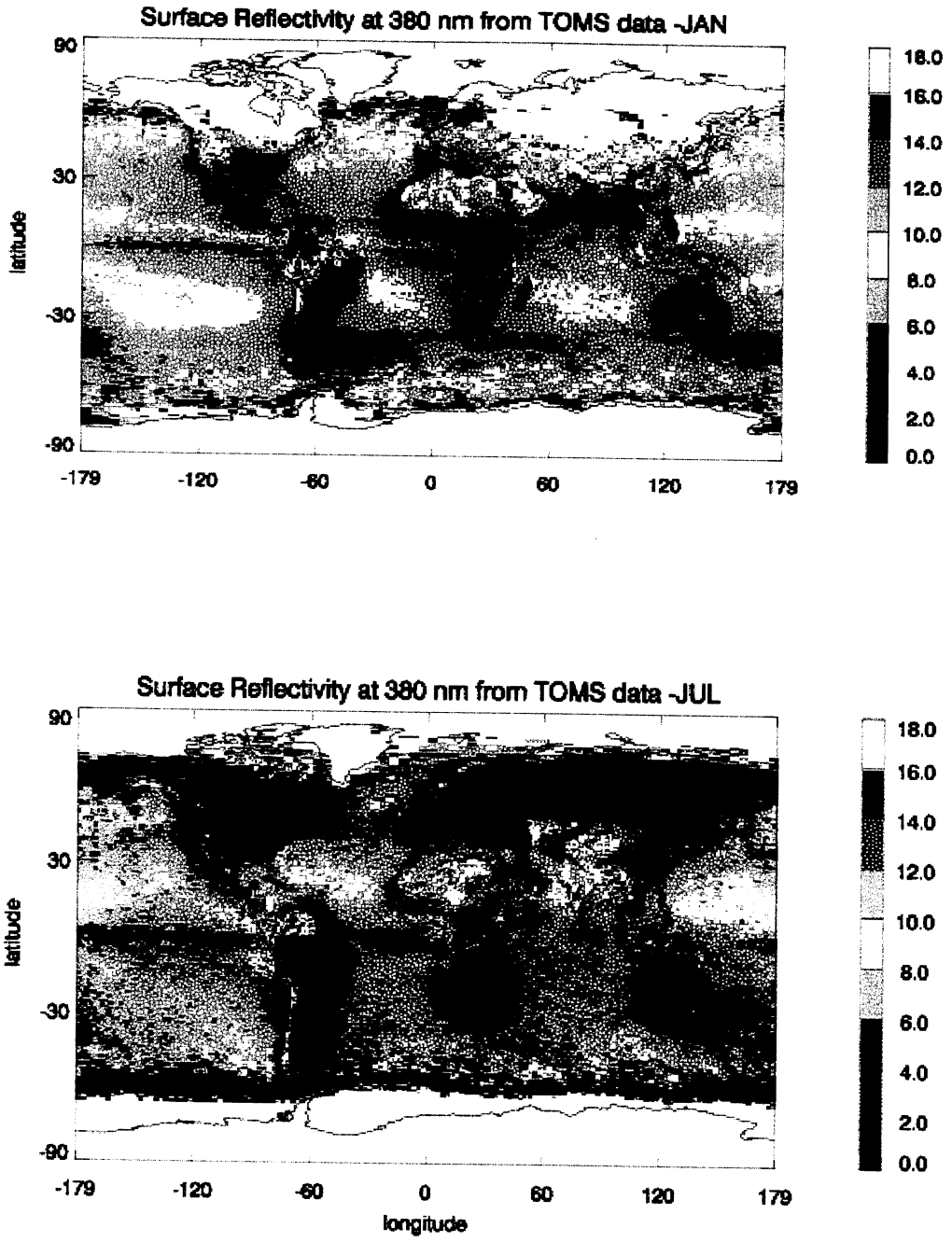

Figure 4 Surface reflectivity measured by TOMS instrument,

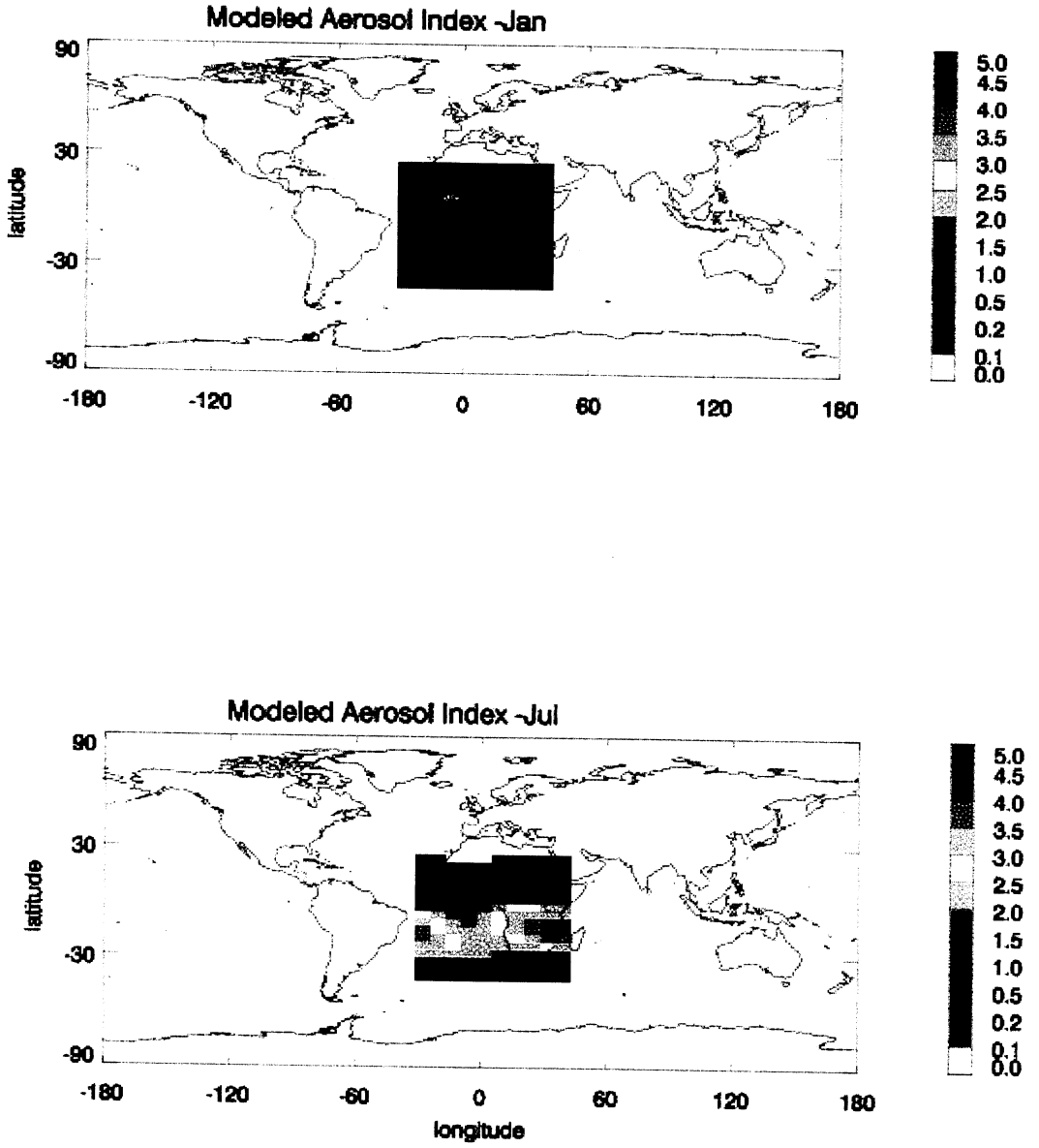

Figure 5. Model simulated aerosol index (AI) in January and July for the region of (30 W, 37.5 E) (42S, 35N). Dust and biomass carbon are included in the calculation.

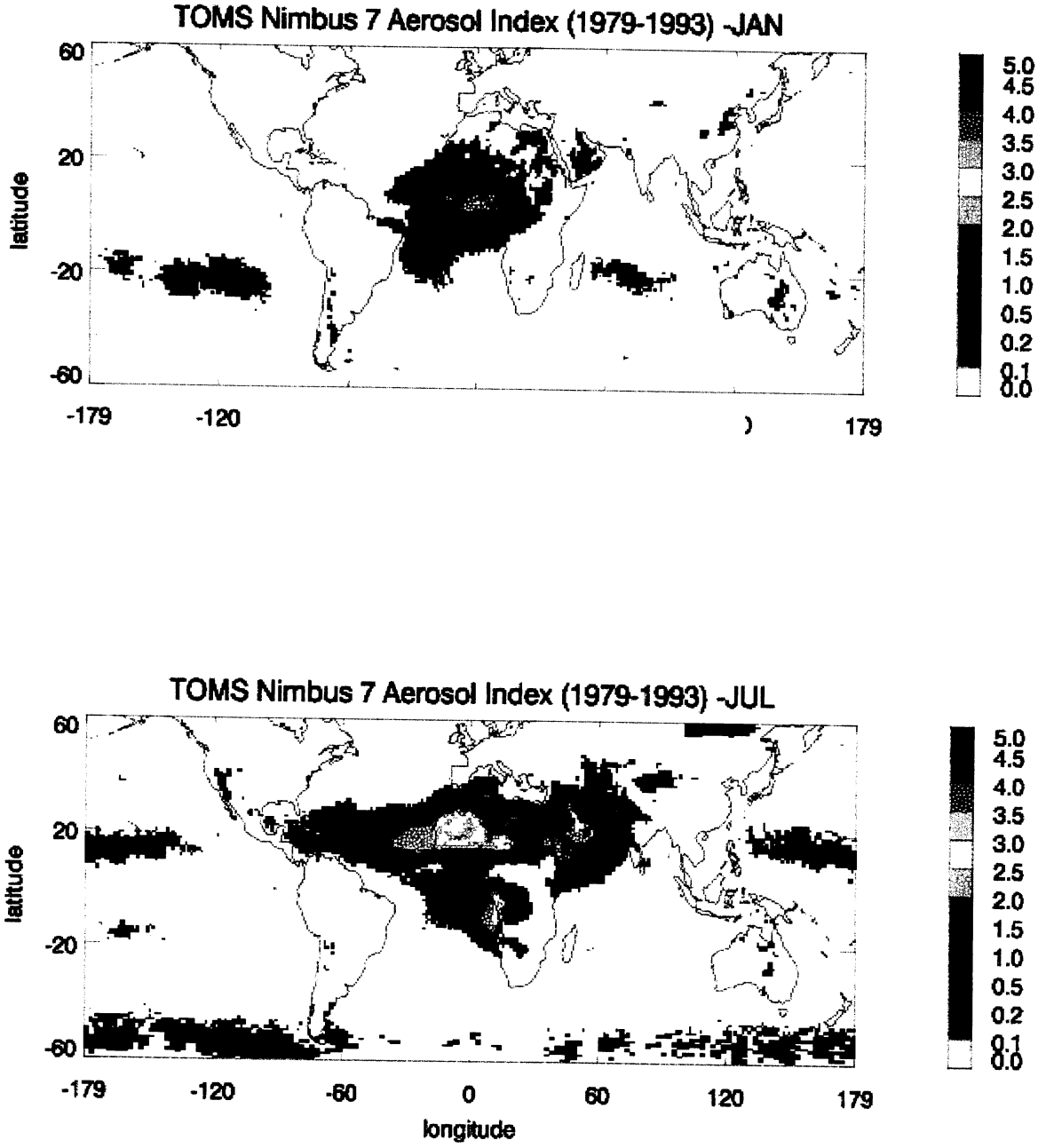

Figure 6. Average Aerosol Index (AI) measured by TOMS Nimbus 7 instrument.